

Determination of the Fermi Velocity by Angle-dependent Periodic Orbit Resonance Measurements in the Organic Conductor α -(BEDT-TTF)₂KHg(SCN)₄

A. E. Kovalev, S. Hill[†]

Department of Physics, University of Florida, Gainesville, FL 32611

J. S. Qualls

Department of Physics, Wake Forest University, Winston-Salem, NC 27109

(November 4, 2018)

We report detailed angle-dependent studies of the microwave ($\nu = 50$ to 90 GHz) interlayer magneto-electrodynamics of a single crystal sample of the organic charge-density-wave (CDW) conductor α -(BEDT-TTF)₂KHg(SCN)₄. Recently developed instrumentation enables both magnetic field (\mathbf{B}) sweeps for a fixed sample orientation and, for the first time, angle sweeps at fixed ν/\mathbf{B} . We observe series' of resonant absorptions which we attribute to periodic orbit resonances (POR) – a phenomenon closely related to cyclotron resonance. The angle dependence of the POR indicate that they are associated with the low temperature quasi-one-dimensional (Q1D) Fermi surface (FS) of the title compound; indeed, all of the resonance peaks collapse beautifully onto a single set of ν/\mathbf{B} versus angle curves, generated using a semiclassical magneto-transport theory for a single Q1D FS. We show that Q1D POR measurements provide one of the most direct methods for determining the Fermi velocity, without any detailed assumptions concerning the bandstructure; our analysis yields an average value of $v_F = 6.5 \times 10^4$ m/s. Quantitative analysis of the POR harmonic content indicates that the Q1D FS is strongly corrugated. This is consistent with the assumption that the low-temperature FS derives from a reconstruction of the high temperature quasi-two-dimensional FS, caused

by the CDW instability. Detailed analysis of the angle dependence of the POR yields parameters associated with the CDW superstructure which are consistent with published results. Finally, we address the issue as to whether or not the interlayer electrostatics are coherent in the title compound. We obtain a relaxation time from the POR linewidths which is considerably longer than the interlayer hopping time, indicating that the transport in this direction *is* coherent.

PACS numbers: 71.18.+y, 72.10.-d, 74.70.Kn, 76.40.+b

I. INTRODUCTION

A detailed knowledge of the Fermi surface (FS) topologies of low-dimensional conductors is an essential starting point for understanding the mechanisms that drive the various electronic instabilities which result in, *e.g.* the magnetism or superconductivity in these systems [1,2]. For example, recent theoretical studies have shown that the symmetry of the superconducting state in quasi-two-dimensional (Q2D) and quasi-one-dimensional (Q1D) systems is extremely sensitive to the nesting characteristics of the FS [3–5]. Furthermore, the organic compound central to this investigation has recently aroused considerable interest due to a range of exotic phenomena which derive from its intrinsic electronic low-dimensionality, *e.g.* multiple field-induced charge density wave (CDW) phases [6], and field-induced dynamic diamagnetism associated with a dissipationless conductivity [7]. Although there exists an extensive array of experimental techniques for probing FS topologies, few possess the necessary resolution to profile the small (often $< 1\%$) deformations (warpings) that arise due to weak dispersion along the low conductivity axis (axes) of Q2D (Q1D) systems.

We have recently developed new methods for determining the FS topologies of quasi-low-dimensional systems using a millimeter-wave spectroscopic technique [8–10]. A novel type of cyclotron resonance (CR) is predicted to occur – the so-called periodic orbit resonance (POR) – which is fundamentally different from the conventional CR observed in

normal metals [8,11–14]. This technique, which was first considered by Osada *et al.* [14], essentially corresponds to high frequency angle-dependent magnetoresistance oscillations (AMRO) [2,11,14]. In this article, we report extensive high sensitivity POR measurements of the organic charge transfer salt α -(BEDT-TTF)₂KHg(SCN)₄ (where BEDT-TTF denotes bis-ethylenedithio-tetrathiafulvalene or ET for short [1,2]). These studies extend the earlier work of Ardavan *et al.* [12]. In particular, the exceptional sensitivity offered by our spectrometer, together with the elimination of all spurious experimental artifacts, enables us to observe many POR harmonics. The use of a split-pair magnet allows in-situ rotation, thereby facilitating extensive angle dependent POR investigations. Consequently, these studies provide a rigorous test of the semiclassical theories commonly used to analyze many aspects of the transport properties of low-dimensional conductors [14–17], and enable a determination of important parameters describing the FS topology of α -(ET)₂KHg(SCN)₄. Furthermore, as we shall show, the POR technique represents one of the most direct and accurate means of measuring the Fermi velocity in Q1D systems; here, we report the first such measurement for a Q1D conductor.

α -(ET)₂KHg(SCN)₄ possesses a layered crystal structure in which the highly conducting ET planes are separated by insulating anion layers [1,2]; for this material, the least conducting direction is along the crystallographic b^* -axis. The ratio of in-plane to interlayer conductivities is about $\sigma_{\parallel}/\sigma_{\perp} \sim 10^5$ (see Refs. [1,2]). Within the conducting layers, the flat donor ET molecules are arranged face-to-face in a herring bone structure. Weak overlap of the sulphur π -orbitals, oriented normal to the planes of the ET molecules, gives rise to a fairly isotropic in-plane conductivity, and to a Q2D band structure which may be calculated using a tight binding approximation [1,2,18].

According to band structure calculations, the FS of this metal consists of a pair of Q1D open sections (corrugated sheets), and a Q2D cylindrical section with the axis of the cylinder perpendicular to the layers (see Fig. 1a) [1,2,18]. At about 8K, α -(ET)₂KHg(SCN)₄ exhibits a phase transition into a low temperature state [19]; this transition is believed to be driven by a nesting instability associated with the Q1D FS, resulting in the formation of a CDW

state [6]. The superstructure associated with the CDW also affects the Q2D FS [20,21]; the reconstructed low-temperature FS again consists of both Q1D and Q2D sections, a possible form of which is shown in Fig. 1b [20]. However, the origin of the low temperature Q1D FS is not related to the underlying lattice symmetry; rather, it is related to the CDW nesting vector. As discussed above, the interplay between the CDW and the residual low-temperature carriers gives rise to several spectacular effects in high magnetic fields [6,7]. Consequently, these investigations provide important insights into this high field behavior.

The article is organized as follows: in the following section, we outline the theoretical background behind the POR phenomenon; in Section III we describe our experimental methods; in Section IV we present the results of our POR measurements on α -(ET)₂KHg(SCN)₄; the results are discussed in Section V; and we end with a summary and conclusions in Section VI.

II. THEORETICAL BACKGROUND

The energy barrier separating the Q1D and Q2D FS sections in Fig. 1b is relatively small: in fields above ~ 10 T, magnetic breakdown occurs, and electrons begin to follow closed orbits corresponding to the original Q2D FS. These closed orbits reveal themselves in the Shubnikov-de Haas (SdH) and de Haas-van Alphen (dHvA) effects [22,23]. The existence of a highly corrugated Q1D FS was first confirmed by AMRO measurements in the limit of zero frequency (DC AMRO) [14,15,24–26], *i.e.* under the condition $\nu \ll \tilde{\nu}_c$, where ν is the measurement frequency and $\tilde{\nu}_c$ is the frequency with which electrons cross the Brillouin zone. These measurements demonstrated that, while rotating magnetic field in a plane perpendicular to the layers, the AMRO exhibit sharp minima.

We briefly discuss the physical origin of the Q1D AMRO effect with reference to the reciprocal space coordinate system defined in Fig. 2a, in which the Q1D FS is parallel to the $k_y k_z$ -plane, and the highly conducting ET layers are parallel to the $k_x k_y$ -plane [27]. Application of a magnetic field causes quasiparticles to follow trajectories perpendicular to

the applied field and parallel to the Q1D FS sheets (yz -plane), as depicted in Figs. 2b and c. This results in periodic modulations of the quasiparticle velocities [$\vec{v} = \hbar^{-1}\nabla_k\varepsilon(k)$, *i.e.* \perp FS], which are most pronounced for the components parallel to the Q1D sheets (v_y and v_z in this case); the resultant real-space trajectory is illustrated in Fig. 2b. The velocity modulations are related to the weak FS corrugations, which may be expressed in terms of Fourier components [14,15]. Each Fourier component has an associated AMRO minimum. This is best illustrated with the aid of Figs. 2b and c, and by considering the semiclassical Boltzmann transport equation [28]: for general quasiparticle trajectories on the Q1D FS (Fig. 2b), v_y and v_z are effectively averaged to zero, and do not contribute appreciably to the conductivity; for special cases in which quasiparticles follow trajectories parallel to a particular corrugation (Fig. 2c), v_y and v_z are *not* effectively averaged to zero – such trajectories contribute maximally to the conductivity, thereby giving rise to the pronounced ρ_y and ρ_z resistivity minima.

Provided that the FS corrugations are weak, all quasiparticle trajectories will be parallel and approximately straight in reciprocal space (not in real space – see Fig. 2b), with their orientations determined solely by the projection of the applied magnetic field onto the plane of the FS (yz -plane) [14,15]; AMRO minima then occur whenever the quasiparticle trajectories run parallel to a particular Fourier component of the corrugations. Thus, the DC AMRO minimum condition depends only on the field orientation relative to the crystallographic (or CDW superstructure) axes, and not on its magnitude. For an orthorhombic crystal, one expects AMRO minima which are periodic in $\tan\theta$, and symmetric about $\theta = 0^\circ$, where θ is the angle between the applied field and the normal to the conducting layers [b^* -axis for α -(ET) $_2$ KHg(SCN) $_4$]. The periodicity is determined by the crystal (or CDW super-) lattice parameters, and scaled by the factor $1/\cos\phi$, which projects the applied magnetic field onto the plane of the FS; ϕ is the azimuthal angle between the yz -plane, and the plane defined by the magnetic field and z -axes (see Fig. 2a). For an oblique lattice, Q1D DC AMRO minima are observed for $\phi = 0$ rotations at angles θ_{mn} given by

$$\tan \theta_{mn} = \left(\frac{m}{n} \times \frac{l}{b^*} \right) + \frac{l'}{b^*}, \quad (1)$$

where b^* is the interlayer spacing, l is the in-plane lattice spacing (parallel to the Q1D FS, or y in this case), and l' is the obliquity parameter defined in Fig. 2d [14,15]. The indices m and n parameterize the Fourier components of the FS corrugations. For α -(ET)₂KHg(SCN)₄, significant DC AMRO minima have only been observed for $n = 0, 1$, and $m = \pm 0, \pm 1, \pm 2, \dots etc.$; θ rotation measurements, performed at several different azimuthal angles ϕ , have enabled determination of the orientation of the Q1D FS sheet relative to the crystallographic axes, and of the ratios l/b^* and l'/b^* which characterize the low temperature CDW [24–26].

The theory of both Q1D and Q2D AMRO has been extended to high frequencies by several authors [8,11–14]; high frequency implies $\nu \sim \tilde{\nu}_c$, *i.e.* when the measurement frequency becomes comparable to the frequency of the periodic k -space orbits. High frequency AMRO, or POR, are closely related to CR. Indeed, DC AMRO represent a limiting case of CR/POR. For the situation depicted in Fig. 2c, the quasiparticle reciprocal space trajectory does not modulate the real space velocity. Consequently, such orbits give rise to a $\nu = 0$ Drude peak in the conductivity, *i.e.* an AMRO minimum [15]. For the situation depicted in Fig. 2b, the quasiparticle reciprocal space trajectories *do* modulate the real space velocity components. Such orbits give rise to finite frequency Drude conductivity peaks. Therefore, although the situation depicted in Fig. 2b does not give rise to a DC AMRO minimum, *it will* give rise to a finite frequency Drude peak in the conductivity when the measurement frequency matches the velocity modulation frequency. In practice, a sample is placed in a microwave resonator, providing a well defined electromagnetic field environment, and resonant absorption occurs whenever the high frequency AMRO/POR condition is met [9]. As in the DC case, each Fourier component of warping produces a distinct POR. However, in contrast to the DC case, the resonance positions (angles) depend on the ratio of the microwave frequency to the external field, *i.e.* ν/B . The resonance condition for the orthorhombic lattice, given in Ref. [11,14], may be generalized for an arbitrary lattice, and for an arbitrary rotation plane,

i. e.

$$\frac{\nu}{B_{res}} = \frac{ev_F}{h} \left[(nb^*)^2 \cos^2 \phi + (ml + nl')^2 \right]^{1/2} |\sin(\theta - \theta_{mn})|, \quad (2)$$

where

$$\tan \theta_{mn} = \frac{1}{\cos(\phi)} \left(\frac{ml}{nb^*} + \frac{l'}{b^*} \right), \quad n = 0, 1, 2, \dots, m = 0, \pm 1, \pm 2, \dots \quad (3)$$

Here, b^* , l , l' , m , n , θ and ϕ have the same definitions as above; v_F is the Fermi velocity, which is assumed to be constant over the entire Q1D FS; and B_{res} represents the applied field strength at which a POR will be observed for a particular pair of indices m and n . Eq. (2) may be further simplified as follows,

$$\frac{\nu}{B_{res}} = \frac{ev_F}{h} \times nb^* \cos \phi \left| \frac{\sin(\theta - \theta_{mn})}{\cos(\theta_{mn})} \right|, \quad n \geq 0. \quad (4)$$

In contrast to the DC case, one can now observe all θ_{mn} resonances by sweeping the magnetic field or frequency with the sample orientation fixed; our experimental set-up permits the former (see following section). One can also carry out angle rotations at fixed ν/B . However, unlike the DC case, where the AMRO minima are determined solely by Eq. (3) [or Eq. (1)], the finite frequency resonances are found from the combined solutions to Eqs. (3) and (4). For a particular ν/B , each DC AMRO minimum splits into two finite frequency branches, having opposite circular polarizations about the x -axis: these result from the positive and negative values of $\sin(\theta - \theta_{mn})$ in Eq. (4); thus, one branch moves to higher angles with increasing ν/B , the other to lower angles. Each branch persists up to a maximum ν/B , at which $(\theta - \theta_{mn}) = \pm 90^\circ$. The form of the angle dependence of the Q1D POR may be seen in Fig. 4 of Refs. [11,12], and in the results section of this article (Fig. 5 below).

In a field swept experiment, several resonances are observed, corresponding to different Fourier components, or harmonics of the warping. Unlike the harmonics observed in conventional CR experiments on Q2D and 3D systems with non-parabolic dispersion [8,11], the Q1D POR harmonics are, in general, not commensurate, *i.e.* they are not evenly spaced in ν/B , as has been noted in previous experiments on Q1D organic conductors [29]. At the DC AMRO minimum angles, however, the harmonics do become commensurate.

There are a number of fitting parameters in Eqs. (2)–(4): in principle, θ and ϕ should be known, though they may also be determined from measurement (see below), and through comparison with DC AMRO data; b^* is known from X-ray data [1]; θ_{mn} and, hence, l and l' may be determined either from θ sweeps at different ϕ and ν/B , or field sweeps at different θ and ϕ . The final fitting parameter, v_F , is more-or-less insensitive to the other fit parameters. Therefore, Q1D POR offers one of the most direct and accurate means of measuring the Fermi velocity in Q1D systems. We note that McKenzie and Moses have proposed an alternative theory to describe Q1D POR in low-dimensional organic conductors [16], though the resonance condition [Eqs. (2)–(4)] turns out to be the same. However, as we will show below, this theory appears to be inappropriate for the case of α -(ET)₂KHg(SCN)₄.

As described above, resonances are expected for the conductivity components parallel to the Q1D FS. More detailed considerations show that, for the case of layered organic conductors, it is preferential to measure the interlayer conductivity – both for the DC case [14], and for POR measurements [8,10]. Under such conditions, only resonances with $n = 1$ are detected, and their amplitudes are proportional to the squares of the Fourier amplitudes (t_{m1}^2) of the FS warping components [11]. The resonance line shape has a Lorentzian form when observed through conductivity measurements; and the resonance line width is given by τ^{-1} , where τ is the relaxation time.

III. EXPERIMENTAL

The high degree of sensitivity required for single crystal measurements is achieved using a resonant cavity perturbation technique in combination with a broad-band Millimeter-wave Vector Network Analyzer (MVNA [30]) exhibiting an exceptionally good signal-to-noise ratio [9]. The MVNA is a phase sensitive, fully sweepable (8 to 350 GHz), superheterodyne source/detection system. For the purposes of these measurements, a waveguide probe, optimized to work in the 40 to ~ 120 GHz range, was used to couple radiation to and from a cylindrical resonator which we operate in transmission mode; the essential details of this instrumentation are described in detail in ref. [9]. In order to enable rotation of the sample relative to the applied magnetic field, we utilize split-pair magnet with a 7 T horizontal field and a vertical access. Smooth rotation of the entire rigid microwave probe, relative to the fixed field, is achieved via a room temperature stepper motor mounted at the neck of the magnet dewar; the stepper motor offers 0.1° angle resolution. The source and detector (harmonic generator and mixer) are bolted rigidly to the microwave probe; subsequent connection to and from the MVNA is achieved via flexible coaxial cables [9]. In this mode of operation, one can maintain optimal coupling between the spectrometer and the cavity containing the sample, *whilst* rotating the probe. As discussed in great detail in ref. [9], good coupling between the various microwave elements is essential in order to maintain a high sensitivity and a low noise level. These factors are the main reason for the vastly improved quality of the POR data presented in the following section, relative to similar previous investigations [12]. Rotation of the entire rigid sample probe also ensures that the sample sits in a reproducible electromagnetic field environment for all measurements made on a particular mode of the cavity.

The sample, which was grown by standard techniques [1], has a platelet shape (\sim dimensions $0.8 \times 0.8 \times 0.17$ mm³) and was suspended in the center of the cylindrical cavity by means of a quartz pillar. The axis of the cylindrical cavity was aligned with the rotation axis, while the sample b^* -axis was oriented perpendicular to this axis, *i.e.* parallel

to the plane of rotation, thereby ensuring fixed ϕ rotations. The $\theta = \pm 90^\circ$ orientations may be determined from fixed field angle sweeps. ϕ rotations were carried out by hand, at room temperature, and recorded using a digital camera attached to a microscope; calibration of ϕ was achieved through subsequent data analysis. The base frequency of the cavity used for these measurements was $\nu = 53.9$ GHz, corresponding to the TE011 cylindrical mode with a Q -factor of about 10^4 . Higher frequency measurements were also performed on higher order modes of the same cavity without the need to warm up the probe. The use of a cavity enables positioning of a single crystal sample into a well defined electromagnetic field environment, *i.e.* the orientations of the DC and AC electromagnetic fields relative to the sample's crystallographic axes are precisely known. In this way, one can systematically probe any diagonal component of the conductivity tensor [10]. In this particular investigation, measurements were restricted to modes which probe only the interlayer electrostatics; the precise details as to how we achieve this are described elsewhere [9,10]. Consequently, the measured absorption is directly proportional to the interlayer conductivity $\hat{\sigma}_{b^*}(\omega, \mathbf{B}, T)$.

All measurements were carried out at a temperature of about 2.2 K. The temperature was stabilized using a Quantum Design PPMS variable flow cryostat. Data were obtained for both field sweeps at constant angle, and angle sweeps at constant field. The data presented in the following section are limited to rotation in two planes corresponding to $\phi=28^\circ$ and $\phi=66^\circ$.

IV. RESULTS

Figure 3 shows the typical microwave absorption curves for field swept measurements at different fixed sample orientations ranging from $\theta = -20^\circ$ to $+5^\circ$ in 5° steps (the traces have been offset for clarity); $\phi = 28^\circ$ in each case, and the data were all obtained at $\nu = 53.9$ GHz (TE011 mode). The most obvious aspect of the data are the peaks in absorption corresponding to peaks in the interlayer conductivity. As we shall now detail, these peaks correspond to PORs. The first point to note is that there is no simple harmonic

relationship between the peak positions (B_{res}) within a given trace, *i.e.* the peaks are incommensurate. Each peak may clearly be associated with a particular POR branch; in other words, there is a smooth shift in the positions of the peaks belonging to each branch, as indicated by the dashed lines. Most notable is the dominant peak in the $\theta = 5^\circ$ data, which splits into two distinct branches upon rotation. One branch moves rapidly to higher fields, while the other branch moves to lower fields with a weaker angle dependence. This angle dependence is completely incompatible with a Q2D CR theory, as has been noted previously by several authors [12,29]. As we shall show below, all of the resonance peaks collapse beautifully onto a single set of ν/B_{res} vs θ curves generated using a Q1D POR theory for a single Q1D FS. As discussed in the previous section, each particular POR branch corresponds to a specific Fourier component of the warping of the Q1D FS, and the resonances in Fig. 3 have been labeled accordingly. The amplitudes of the peaks are only weakly angle dependent; we discuss the relative intensities of the peaks further below. The quality of the data in Fig. 3 is unprecedented for a measurement in this frequency range; indeed, this data is of comparable quality to the best DC measurements.

Figure 4 shows microwave absorption for fixed ν/B θ -sweeps, at an azimuthal angle $\phi=28^\circ$. These data were again obtained using the TE011 mode of the cavity, while varying ν/B by means of the applied field strength (indicated in the figure). Once again, several clear absorption peaks are observed corresponding to distinct PORs. In fact, each trace is highly reminiscent of DC AMRO data [14,15,24–26], albeit inverted, *i.e.* conductivity peaks are seen in POR measurements, whereas resistivity minima are observed in AMRO experiments. However, closer inspection indicates that the POR peak positions clearly depend on the field strength, in marked contrast to the DC AMRO case. Once again, each peak belongs to a POR branch corresponding to a particular Fourier component of the FS warping, and several of the branches have been labeled accordingly in Fig. 4. The noise level is slightly higher in Fig. 4, when compared to Fig. 3. This is attributable to unavoidable mechanical vibrations associated with the rotation of the probe. Thus, the field swept measurements are intrinsically cleaner. However, the signal-to-noise ratio is still exceptionally good, even in

the angle swept mode. It is also somewhat easier to observe higher order (higher $|m|$) POR in this mode of operation, by sweeping through angles close to $\theta = \pm 90^\circ$ at the maximum field of $\sim 7\text{T}$. At lower fields, the condition $2\pi\tilde{\nu}\tau = \tilde{\omega}\tau \sim 1$ is not met for many of the higher m modes, as evidenced by the disappearance of the closely spaced peaks around $\theta = 90^\circ$ in the lower field data in Fig. 4.

In Fig. 5, we compile all of the $\phi=28^\circ$ field swept data into a single plot of ν/B_{res} versus θ , where the data points represent the peak positions, B_{res} , obtained from data similar to those in Fig. 3. Fig. 5 includes measurements performed at two separate frequencies: $\nu = 53.9\text{ GHz}$ (open circles) and $\nu = 89.2\text{ GHz}$ (solid triangles). The data collapse onto a set of $\sin(\theta - \theta_{mn})$ arches according to Eqs. (2) and (4). All of the resonances may be labeled using a single index m , as is also the case for DC AMRO measurements [15,24–26]. The dotted lines are fits according the Eqs. (3) and (4); the exceptional quality of the fits may be attributed to the high quality of the measurements. Qualitative comparisons of the intensities of the peaks reveal that they scale approximately with $\cos \theta_{mn}$, *i.e.* the resonances with zero field intercepts closest to $\theta = 0^\circ$ ($m = 0$ and 1 Fig. 5) have the strongest intensities.

In order to compare data obtained for different rotation planes (different ϕ), we expand the $\sin(\theta - \theta_{mn})$ term in Eq. (4), giving

$$\frac{\nu}{B_{res} \cos \theta} = \frac{e v_F}{h} \times b^* \cos \phi |\tan \theta_{mn} - \tan \theta|, \quad (5)$$

where we have set $n = 1$. Thus, plots of $\nu/(B_{res} \cos \theta)$ versus $\tan \theta \cos \phi$ should produce straight lines of slope $\pm e b^* v_F/h$, with offsets given by θ_{mn} . Such a plot is shown in Fig. 6, for all of the data obtained from these investigations, *i.e.* both field and angle sweeps, and for two rotation planes ($\phi = 28^\circ$ and $\phi = 66^\circ$). We see that the data collapse very nicely onto the theory over most of the angle range. Deviations from the theory may be mainly attributed to small errors associated with the calibration of the true angle θ ; the nature of the theory amplifies these errors for angles close to $\theta = 90^\circ$, *i.e.* data close to the edges of

Fig. 6.

From the fits in Figs. 5 and 6, we can extract a Fermi velocity for the Q1D Fermi surface of about $v_F = 6.5 \times 10^4 m/s$. In principle, the same value could be estimated from the data in Ref. [12]. This value for the Fermi velocity is very close to the value obtained from fits to optical conductivity data using a Drude model [31]. It should be stressed, however, that our measurements give the most straightforward determination of the Fermi velocity; the only assumption that is made is that the PORs are due to the semiclassical motion of quasiparticles on a Q1D FS – no assumptions about the details of the band structure are required! Nevertheless, this represents an average value, *i.e.* we have assumed a constant Fermi velocity over the entire FS. We shall comment on the validity of this assumption in the following section.

The ratios l/b^* and l'/b^* obtained from our data are 1.2 and 0.5 respectively. These values are in excellent agreement with those obtained from DC AMRO [24–26]: $l'/b^* \approx 0.5$, $l/b^* = 1.25–1.35$. Using the theoretical prediction for the line shape [14,11], we can estimate the relaxation time $\tau = 1.5 \times 10^{-11}$ s, which is approximately the same for all peaks. This value is rather high in comparison to the typical τ values derived from a Dingle analysis of SdH and dHvA oscillations. However, similar discrepancies have been noted in the past from POR data obtained for other Q2D organic conductors [8]. The differences may be attributed to sample inhomogeneities, which give rise to additional damping of SdH/dHvA oscillations. This damping is incorporated into the theory of the SdH and dHvA effects as an effective scattering time [32]. Consequently, Dingle analysis likely under estimates τ significantly.

V. DISCUSSION

Comparisons between our data and those obtained by Ardavan *et al.* [12], reveal considerable advantages to our technique. The rotating cavity design utilized by Ardavan *et al.* offers the main benefit that it may be used in axial high field magnets providing fields of up to 45 tesla at the National High Magnetic Field Laboratory (NHMFL) in Florida [33].

However, the split-pair configuration offers many other important advantages that outweigh the high field capability. In particular, the use of a rigidly coupled probe results in a marked improvement in sensitivity (Q -factors of up to 25,000), and a significant reduction in noise [9]. Furthermore, data acquisition is possible whilst simultaneously rotating the field. Gold plating of the waveguides at the high field end of the probe also eliminates spurious magnetic resonances associated with contaminants [9]; these are dramatically apparent in the data in Ref. [12], thereby obscuring important details of the POR measurements. All of these factors add up to a marked improvement in the quality of the results presented here, in comparison to previously published measurements on α -(ET)₂KHg(SCN)₄. This has enabled us to carry out the most detailed magneto-optical investigation of the complex low-temperature phase of this material to date.

The observation of a strong harmonic content to the POR implies that the FS is strongly corrugated, thereby suggesting comparable transfer integrals between neighboring and more distant molecules. This conclusion contradicts the fact that band structure is well described by a tight binding approximation. However, as pointed out in the introduction, the low temperature Q1D FS in α -(ET)₂KHg(SCN)₄ results from a reconstruction of the high temperature FS obtained from tight-binding calculations [20,21]. The reconstruction is caused by the fairly weak superstructure associated with a low temperature CDW transition, *i.e.* the Q1D FS is essentially pieced together from sections of the original high temperature Q2D closed FS. Thus, the transfer integrals that one could deduce from the POR data do not characterize the tight binding nature of the FS. Rather, they characterize the CDW nesting vector and the original Q2D FS. Indeed, the Fermi velocity obtained from these measurements corresponds precisely to the Q2D Fermi velocity in the high temperature state.

We mentioned above, that the POR peak amplitudes are about the same for resonances having the same $|\cos \theta_{mn}|$. This implies that the POR peak amplitudes are closely related to the FS corrugation wavevectors $Q \sim b^*/|\cos \theta_{mn}|$. Comparisons between the $m = 0, 1$ POR peaks, with the $m = 2, -1$ peaks, reveals a roughly factor of 6 difference in amplitude,

while the difference in $|\cos \theta_{mn}|$ is about 2 for these resonances. As pointed out in Section II, the POR amplitudes should scale as the squared Fourier amplitudes associated with the FS corrugation. We note that, for the most extreme form of warping (a square wave), the POR amplitudes would scale as $1/Q^2$. Consequently, the 1/6 difference in amplitude between PORs corresponding to FS warping components differing in Q by a factor of 2, indicates that the corrugation is close to this extreme limit. Thus, it is possible that a reconstruction along the lines discussed in Ref. [21] offers the most realistic description for the low temperature FS in α -(ET)₂KHg(SCN)₄. Due to the strong corrugation, it is quite likely that our assumption of a constant Fermi velocity over the Q1D FS breaks down to some extent. Furthermore, the theory for the POR developed in section II is only approximate when the FS warping is strong. However, deviations from this theory are only likely to be significant when the magnetic field is tilted appreciably out of the plane of the Q1D FS (see Ref. [15]), which may offer an alternative explanation for the deviations between theory and experiment at the edges of Fig. 6.

McKenzie and Moses have published an alternative theory for POR [16]. However, this theory predicts strong so-called "Danner oscillations" (see refs. [17,34]) for field rotations close to $\theta = 90^\circ$ in the $\phi = 90^\circ$ plane, *i.e.* the rotation plane perpendicular to the Q1D FS; these oscillations have never been observed in α -(ET)₂KHg(SCN)₄. This theory also predicts a strong angle dependence of the POR amplitudes for all but the $m = 0$ harmonic, which also contradicts our results. However, McKenzie and Moses raise the important question as to whether interlayer transport should be coherent in order to observe POR and AMRO [17]. This question has since been re-addressed by numerous authors (see *e.g.* [35]). We believe that coherent interlayer transport is not a necessary condition. Within the tight binding approximation, there should be no difference whether one considers "hopping" between layers, or coherent motion; in both of the cases, only the orbital overlaps between nearest neighbor molecules is important.

If one assumes that the interlayer transport is "weakly incoherent" (according to the definition of McKenzie [17]), then energy and in-plane momentum should be conserved for

interlayer hopping. For the sake of simplicity, we consider this situation for the case of a magnetic field rotated in the zy -plane, *i.e.* parallel to the Q1D FS. In the presence of both the DC magnetic field, and an electromagnetic field, the conservation equations are:

$$E^f - E^i = h\nu = \hbar v_F (k_x^f - k_x^i) \cdot \text{sign}(k_x) \quad (6)$$

and

$$\hbar \mathbf{k}_{\parallel}^i + e \mathbf{A}_{\parallel}^i = \hbar \mathbf{k}_{\parallel}^f + e \mathbf{A}_{\parallel}^f, \quad (7)$$

where E is the quasiparticle energy; $\hbar \mathbf{k}_{\parallel}$ is the quasiparticle momentum parallel to the layers; \mathbf{A}_{\parallel} is the component of the magnetic vector potential parallel to the layers at the site of the hopping; and the superscripts i and f denote the initial and final energy, momentum, *etc.*. Because the magnetic field only has B_z and B_y components, one may choose a gauge in which A_x is the only non-zero component of the vector potential, *i.e.* $A_x = B_y z - B_z y$. The change in the vector potential for interlayer hopping is then $A_x^f - A_x^i = B_y b^* - B_z (ml + l')$, leading to

$$\nu = v_F \frac{e}{\hbar} |A_x^f - A_x^i| = \frac{e v_F B}{\hbar} |b^* \sin \theta - (ml + l') \cos \theta| \quad (8)$$

which is equivalent to the Eq. (5). Consequently, the only way to check whether the interlayer transport is coherent is to compare the interlayer hopping rate τ_h ($= \hbar/t_{\perp}$), with the relaxation time τ obtained from the POR linewidths. An estimation of the interlayer transfer integral from the known conductivity anisotropy gives $t_{\perp} \sim 1$ meV, leading to $\tau/\tau_h \sim 20$, indicating that the interlayer transport *is* coherent. The factor of 10 or so difference between the scattering times deduced from magneto-optical studies, and from SdH or dHvA measurements, raises some important issues. We believe that the scattering times deduced

from SdH and dHvA measurements can be misleading, since they do not necessarily reflect the true short-range inelastic scattering time. As discussed above, this may be caused by the effects of sample inhomogeneities on the SdH/dHvA oscillation amplitudes, which are indistinguishable from the effects of real scattering processes [32].

VI. SUMMARY AND CONCLUSIONS

We have presented detailed angle-dependent POR measurements for the organic CDW conductor α -(ET)₂KHg(SCN)₄. In particular, we demonstrate the huge potential of angle swept POR measurements. The quality of our data is unprecedented for measurements in this high frequency range; indeed, it is of comparable quality to the best DC measurements. Extensive angle dependent measurements confirm that the POR are associated with the low temperature Q1D FS; indeed, all of the resonance peaks collapse beautifully onto a single set of ν/\mathbf{B} versus angle curves, generated using a semiclassical magneto-transport theory for a single Q1D FS. Quantitative analysis of the POR harmonic content indicates that the Q1D FS is strongly corrugated, a fact that is consistent with the assumption that the low-temperature FS derives from a reconstruction of the high temperature quasi-two-dimensional FS. Extrapolations of our data to zero frequency reveal good agreement with published DC AMRO measurements.

We argue that Q1D POR measurements provide one of the most direct methods for determining the Fermi velocity in Q1D systems – our analysis yields an average value of $v_F = 6.5 \times 10^4$ m/s. Furthermore, we show that POR is possible both for coherent and incoherent interlayer transport. However, based on the Mott-Ioffe-Regel, the interlayer transport appears to be coherent in this compound, *i.e.* $\tau/\tau_h \sim 20$.

VII. ACKNOWLEDGEMENTS

We thank S. Khan and N. Bushong for assistance. This work was supported by the National Science Foundation (DMR0196461 and DMR0196430). S. H. would like to thank the Research Corporation for financial support.

VII. REFERENCES CITED

[†] email: hill@phys.ufl.edu

- [1] T. Ishiguro, K. Yamaji, and G. Saito, *Organic Superconductors*, Springer-Verlag (Berlin, 1998).
- [2] J. Singleton, Rep. Prog. Phys. **63**, 1111 (2000).
- [3] Y. Tanuma, K. Kuroki, Y. Tanaka, R. Arita, S. Kashiwaya, H. Aoki, cond-mat/0204409.
- [4] T. Kuwabara, M. Ogata, Phys. Rev. Lett. **85**, 4586 (2000).
- [5] T. Takimoto, Phys. Rev. B **62**, R14641 (2000).
- [6] N. Harrison, Phys. Rev. Lett. **83**, 1395 (1999).
- [7] N. Harrison, C. H. Mielke, A. D. Christianson, J. S. Brooks, and M. Tokumoto, Phys. Rev. Lett. **86**, 1586 (1999).
- [8] S. Hill, Phys. Rev. B **55**, 4931 (1997).
- [9] M. Mola, S. Hill, M. Gross, and P. Goy, Rev. Sci. Instrum. **71**, 186 (2000), and references therein.
- [10] S. Hill, Phys. Rev. B **62**, 8699 (2000).
- [11] S. J. Blundell, A. Ardavan, and J. Singleton, Phys. Rev. B **55**, R6129 (1997).

- [12] A. Ardavan, J. M. Schrama, S. J. Blundell, J. Singleton, W. Hayes, M. Kurmoo, P. Day, P. Goy, Phys. Rev. Lett. **81**, 713 (1998).
- [13] A. Ardavan, S. J. Blundell, and J. Singleton, Phys. Rev. B **60**, 15500 (1999).
- [14] T. Osada, S. Kagoshima, N. Miura, Phys. Rev. B **46**, 1812 (1992).
- [15] S. J. Blundell and J. Singleton, Phys. Rev. B **53**, 5609 (1996).
- [16] Ross H. McKenzie and Perez Moses, Phys. Rev. B **60**, R11241 (1999).
- [17] Perez Moses and Ross H. McKenzie, Phys. Rev. B **60**, 7998 (1999); see also R.H. McKenzie and P. Moses, Phys. Rev. Lett. **81**, 4492 (1998).
- [18] H. Mori, S. Tanaka, M. Oshima, G. Saito, T. Mori, Y. Maruyama and H. Inokuchi, Bull. Chem. Soc. Jpn. **63**, 2183 (1990).
- [19] T. Sasaki, N. Toyota, M. Tokumoto, N. Kinoshita, and H. Anzai, Solid State Commun., **75**, 93 (1990).
- [20] M. V. Kartsovnik, A. E. Kovalev and N. D. Kusch, J. Physique I **3**, 1187 (1993).
- [21] N. Harrison, E. Rzepniewski, J. Singleton, P. J. Gee, M. M. Honold, P. Day and M. Kurmoo, J. Phys. Condens. Matter **11**, 7227 (1999).
- [22] T. Osada, R. Yagi, A. Kawasumi, S. Kagoshima, N. Miura, M. Oshima, and G. Saito, Phys. Rev. B **41**, 5428 (1990).
- [23] T. Sasaki, A. G. Lebed, T. Fukase, and N. Toyota, Phys. Rev. B. **54**, 12969 (1996), and references therein.
- [24] A. E. Kovalev, M. V. Kartsovnik, R. P. Shibaeva, L. P. Rozenberg, I. F. Schegolev, N. D. Kusch, Solid State Commun. **89**, 575 (1994).
- [25] Y. Iye, R. Yagi, N. Hanasaki, S. Kagoshima, H. Mori, H. Fujimoto and G. Saito, J. Phys. Soc. Jpn. **63**, 674 (1994).

- [26] J. Caulfield, S. J. Blundell, M. S. L. du Croo de Jongh, P. T. J. Hendriks, J. Singleton, M. Doporto, F. L. Pratt, A. House, J. A. A. J. Perenboom, W. Hayes, M. Kurmoo and P. Day, *Phys. Rev. B* **51**, 8325 (1995).
- [27] In Fig. 2a, the z -axis coincides with the crystallographic b^* -axis for α -(ET)₂KHg(SCN)₄, and the xy -plane coincides with the highly conducting ac -planes. The orientations of the x and y axes relative to the crystallographic a and c directions depends explicitly on the CDW superstructure; it has been shown that the plane of the Q1D FS sheets (yz -plane in Fig. 2) is inclined $\sim 26.6^\circ$ to the crystallographic b^*c -plane [26].
- [28] J. M. Ziman, *Principles of the Theory of Solids* (Cambridge University Press, Cambridge 1972).
- [29] Stephen Hill, M. Mola, J. S. Brooks, M. Tokumoto, N. Kinoshita, T. Kinoshita and Y. Tanaka, in *Physical Phenomena in High Magnetic Fields - III*, edited by Z. Fisk, L. P. Gor'kov and J. R. Schrieffer, p218 (World Scientific, Singapore 1999).
- [30] Produced by AB Millimetre, 52 Rue Lhomond, 75 005, Paris, France; www.abmillimetre.com.
- [31] M. Tamura, R. Masuda, T. Naito, H. Tajima, H. Kuroda, and A. Kobayashi, *Synth. Met.*, **41-43**, 2499 (1991).
- [32] D. Shoenberg, *Magnetic Oscillations in Metals* (Cambridge University Press, Cambridge, 1984).
- [33] We note that a high field split-pair magnet is currently under construction at the NHMFL, which will enable extension of these methods to much higher fields in future.
- [34] G. M. Danner and P. M. Chaikin, *Phys. Rev. Lett.* **72**, 4690 (1995).
- [35] John Singleton, P. A. Goddard, A. Ardavan, N. Harrison, S. J. Blundell, J. A. Schlueter, and A. M. Kini, *Phys. Rev. Lett.* **88**, 37001 (2002).

Figure captions

Fig. 1a) Room temperature FS of α -(ET)₂KHg(SCN)₄ according to the calculation in Ref. [18]. Below 8 K, this FS undergoes a reconstruction, as shown in b); the reconstruction is caused by the superstructure, with characteristic wavevector Q , associated with the low-temperature CDW [20].

Fig. 2a) Definition of the angles θ and ϕ , defining the magnetic field (\mathbf{B}) orientation relative to the Q1D FS within the reciprocal space coordinate system discussed in the main text; the Q1D FS is parallel to the $k_y k_z$ -plane, and the normal to the highly conducting layers (b^* -axis) is parallel to k_z . b) A schematic of a typical quasiparticle trajectory in reciprocal space for a magnetic field applied at an arbitrary angle θ away from the k_z axis, within the plane of the Q1D FS ($k_y k_z$ -plane); the motion of the quasiparticle across the FS corrugations results in a periodic modulation of the real space velocity, v_R (see text for discussion). c) At certain applied field orientations, the quasiparticle trajectories follow constant real-space-velocity contours; these angles correspond to the θ_{mn} AMRO minima (see text). d) The oblique real-space crystal lattice, defining the CDW superstructure within the plane parallel to the Q1D FS; b^* is the interlayer spacing, l and l' are defined in the text.

Fig. 3. Microwave absorption curves for field swept measurements at different fixed sample orientations (indicated in the figure); the temperature is 2.2 K, and the traces have been offset for clarity. The POR have been labeled with the appropriate value of the index m .

Fig. 4. Microwave absorption for fixed ν/B θ -sweeps (offset for clarity), at an azimuthal angle $\phi=28^\circ$. ν/B was varied by means of the applied field strength (indicated in the figure); the measurement frequency was 53.9 GHz and the temperature was 2.2 K. The POR have been labeled with the appropriate value of the index m .

Fig. 5. A compilation of the angle dependence of all of the $\phi=28^\circ$ field swept data, where the data points represent the peak positions, B_{res} , obtained from plots similar to Fig. 3; measurements at two frequencies are included in the figure. Several of the POR branches have been labeled with the appropriate value of the index m .

Fig. 6. A compilation of all of the data obtained in this investigation, scaled according to Eq. (5). Several of the POR branches have been labeled with the appropriate value of the index m .

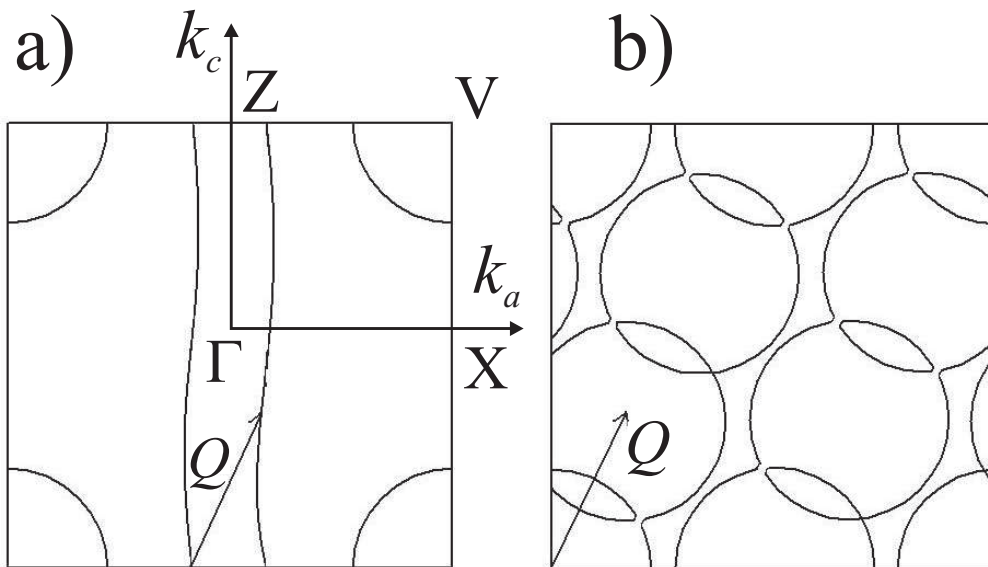


FIG. 1. Kovalev *et al.*

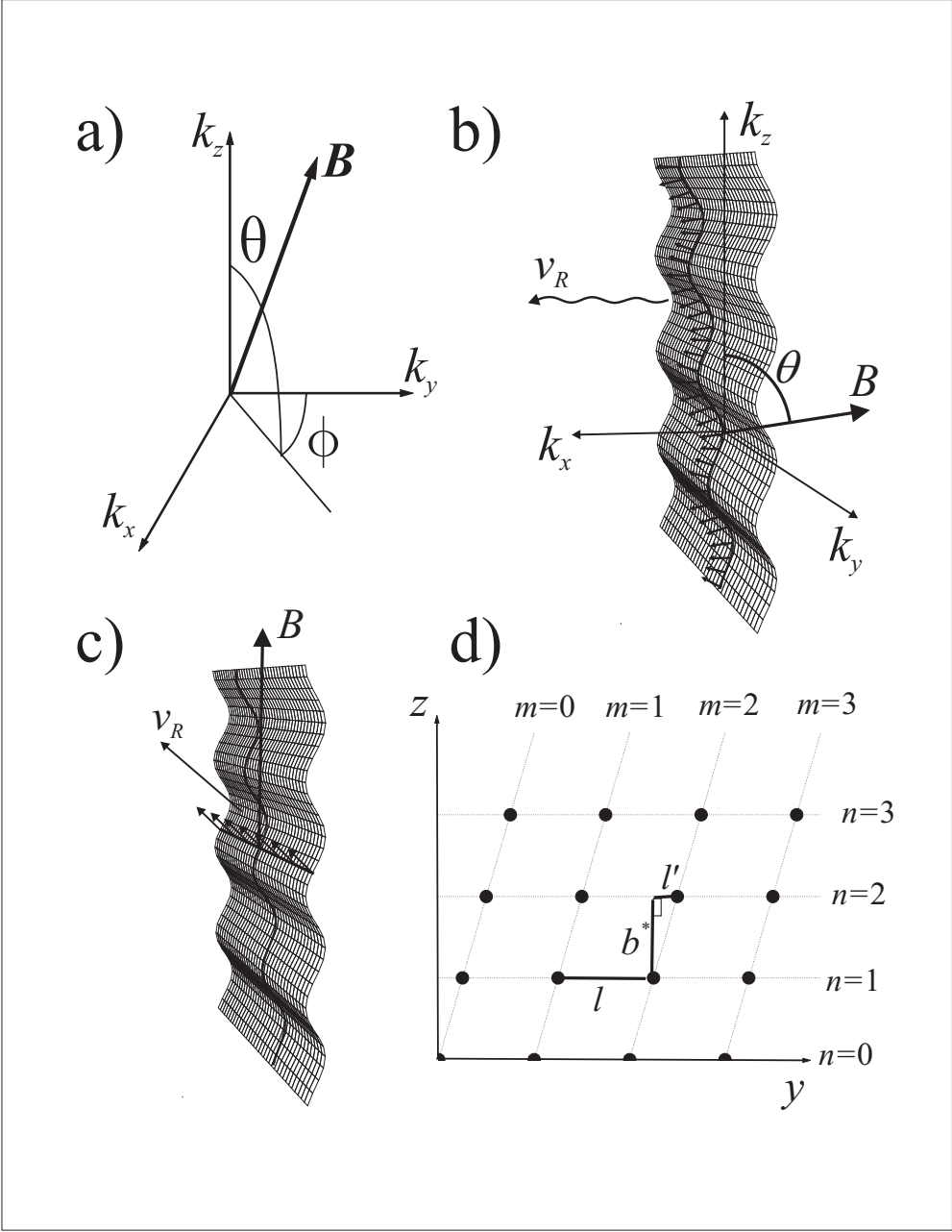


FIG. 2. Kovalev *et al.*

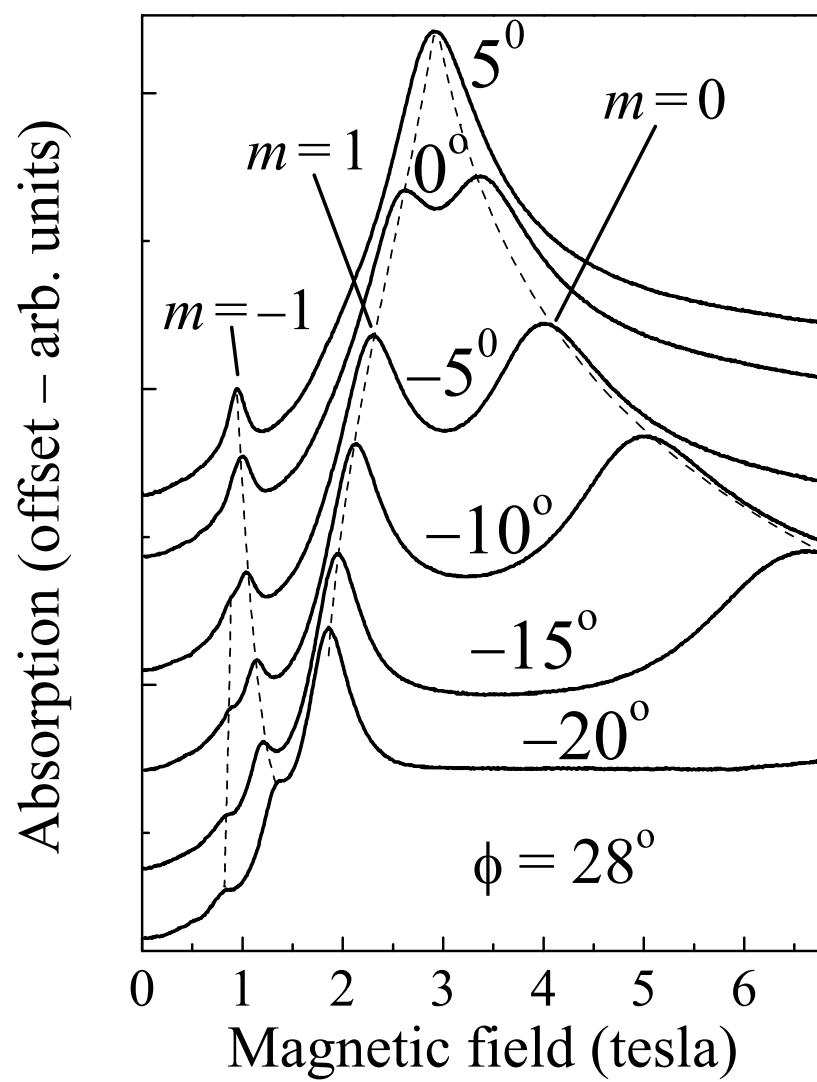


FIG. 3. Kovalev *et al.*

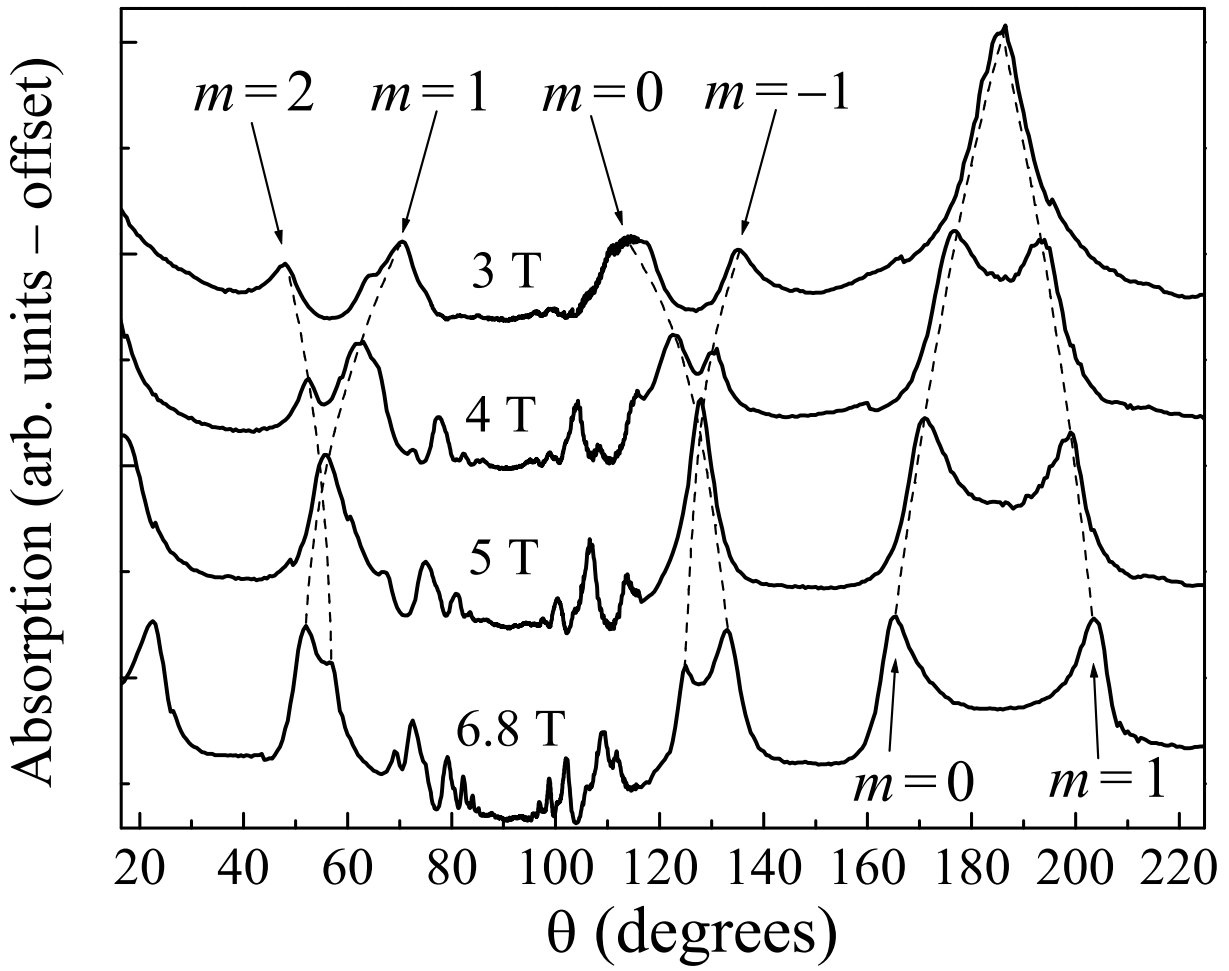


FIG. 4. Kovalev *et al.*

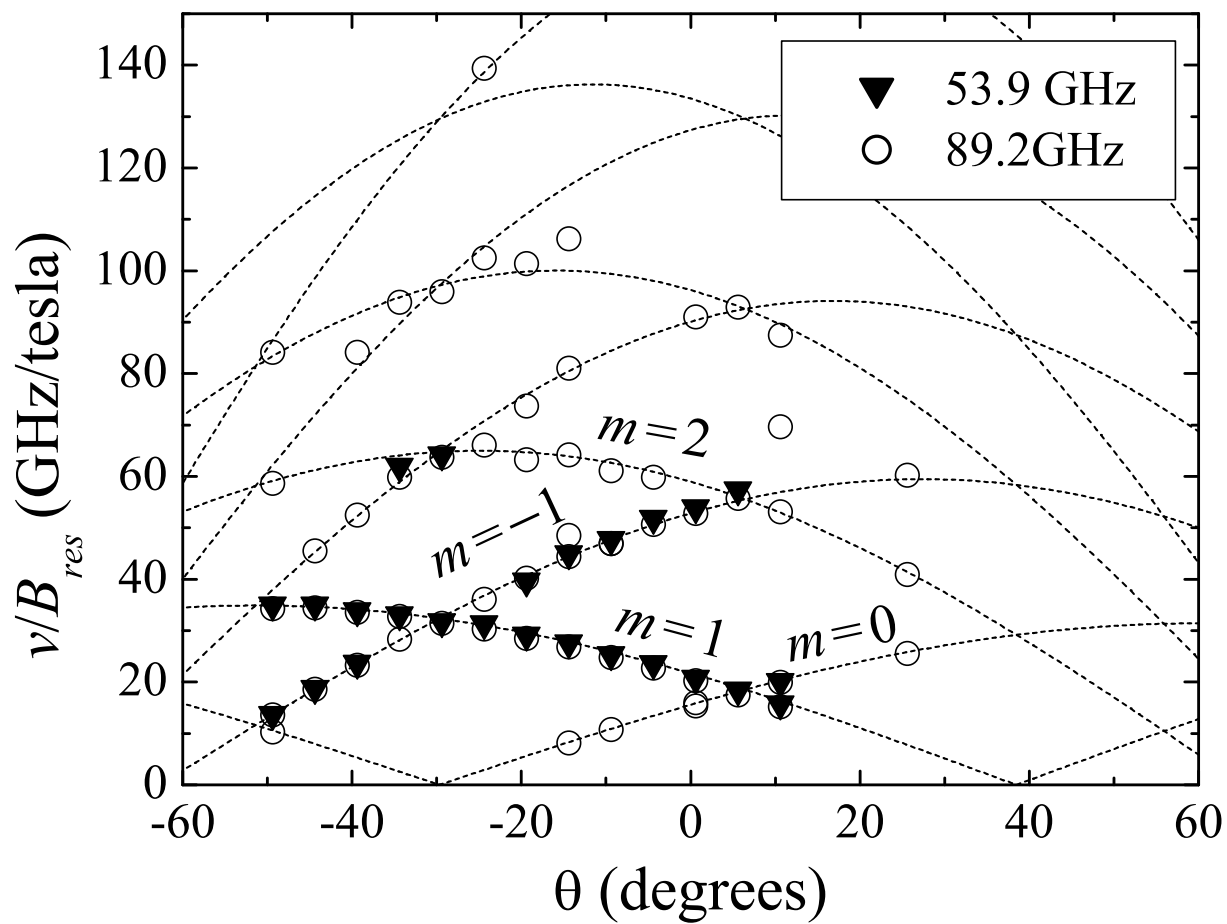


FIG. 5. Kovalev *et al.*

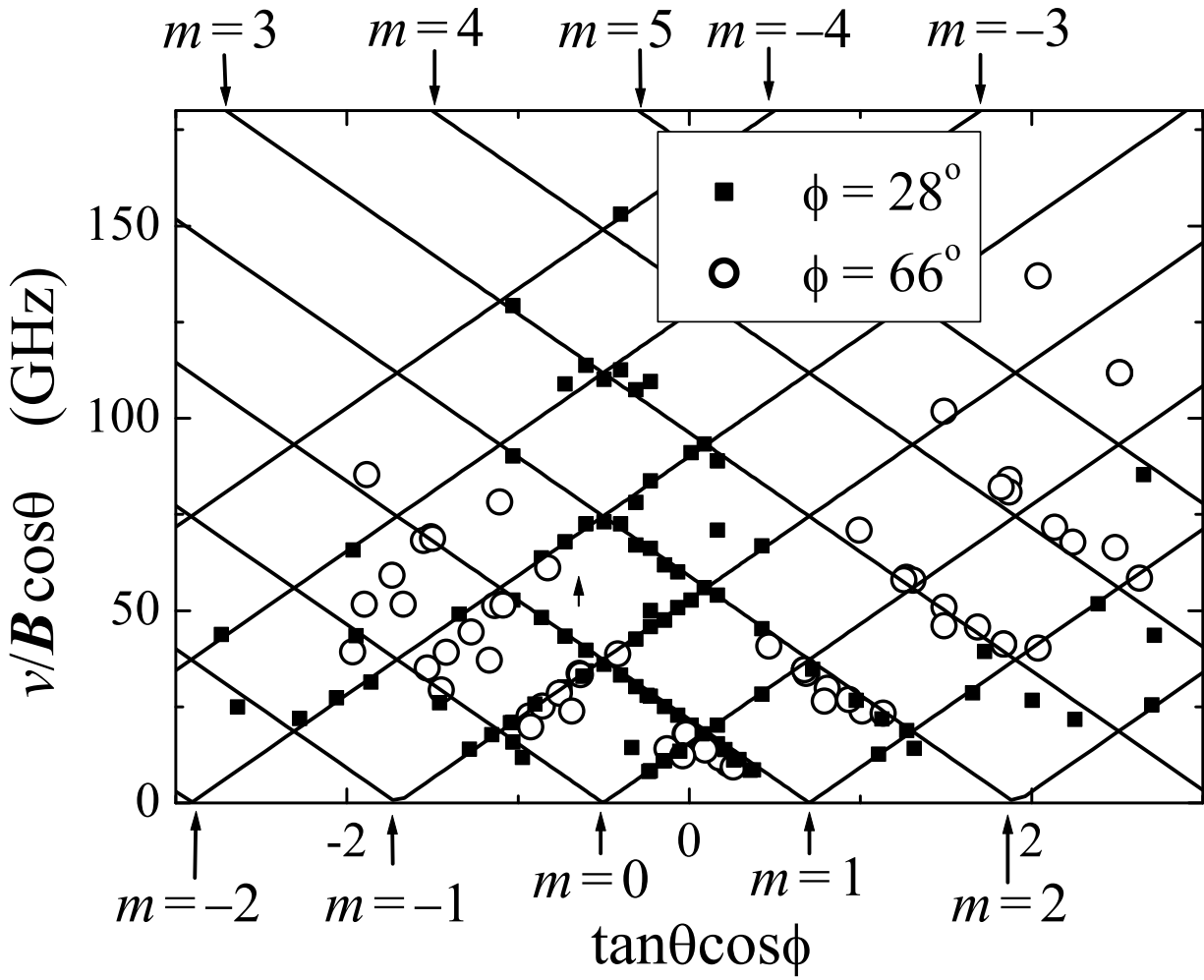


FIG. 6. Kovalev *et al.*